RESEARCH ARTICLE

Testbed for a Novel Approach to Minimizing the PAPR of 5G Systems

SIVAPRASAD VALLURI[1], **CHAKRAVARTHY GUNTURU**[1], **SOWBHAGYA APPALLA**[1], **ANUPAM KAJALE**[1], **AND V. V. MANI**[2], **(Senior Member, IEEE)**

[1]Electronics and Communication Engineering Department, Indian Institute of Information Technology Design and Manufacturing at Kurnool, Kurnool, Andhra Pradesh 518007, India

[2]Electronics and Communication Engineering Department, National Institute of Technology, Warangal, Hanamkonda, Telangana 506004, India

Corresponding author: Sivaprasad Valluri (vsp@iiitk.ac.in)

ABSTRACT The generalized frequency division multiplexing (GFDM) system has attracted the interest of the research community due to its unique characteristics such as high spectrum efficiency, low latency, and high transmission rate. However, like every multicarrier technique superimposition of a number of subsymbols in the time domain results in a high peak-to-average power ratio (PAPR). In general, the PAPR reduction system in the literature increases the average power while decreasing the PAPR which is not a plausible solution for practical 5G applications. In order to address this issue, we propose an efficient PAPR reduction strategy that maintains the PAPR without increasing the average power. In this method, an optimal orthogonal precoding matrix based on singular value decomposition (SVD) is designed to reduce the system's average power. Because this optimal precoding matrix cannot successfully reduce the PAPR, we introduce a second technique called peak samples affixing to minimize both the peak and average power. For the proposed method's assessment, using LabVIEW software and the universal software radio peripheral 2953R (USRP) as hardware, we developed an experimental setup to enable real-time transmission. The received spectral response from USRP authenticated the proposed method by showing a good agreement with simulations.

INDEX TERMS GFDM, PAPR, spectrum, USRP.

I. INTRODUCTION

The current generation has been compelled to boost its throughput efficiency due to the proliferation of smartphones with massive storage capabilities and data-hungry applications [1]. Orthogonal frequency division multiplexing (OFDM) is now widely employed as a physical layer technology due to its exceptional qualities, such as single tap equalization and cost-effective implementation [2]. These benefits come at the expense of strict synchronization, orthogonality, and high power consumption [3]. Apart from high data rates, applications that do not require human intervention, such as machine-type communication (MTC), the Internet of Things (IoT), and vehicle-to-vehicle communication (V2V), are being addressed for future generation system design.

The associate editor coordinating the review of this manuscript and approving it for publication was Mauro Fadda.

These applications entail low power consumption, reduced latency, and asynchronous data transmission [4].

This spurred the exploration of novel physical layer waveforms, which resulted in a multitude of alternative waveforms being presented. Generalized frequency division multiplexing (GFDM), a flexible multi-carrier transmission strategy, would suit the aforementioned characteristics and could be considered a viable contender for the implementation of 5G networks [5]. The GFDM system is based on the modulation of distinct time-frequency blocks, each of which contains several subcarriers in frequency and subsymbols in time. The subcarriers on each subsymbol are filtered with an application-specific prototype filter that is circularly shifted in time and frequency [6]. Together with tail biting, this approach minimizes undesired out-of-band (OOB) emissions and latency [7]. Furthermore, the adaptability of GFDM allows it to handle well-known OFDM and single carrier

frequency domain equalization (SC-FDE) as corner cases [8]. GFDM, like other multicarrier schemes, suffers from a high peak-to-average power ratio (PAPR) issue due to the existence of numerous symbols in the time domain [9].

In GFDM-based systems, there are three main categories of PAPR reduction techniques [10]. The initial and most basic category is signal distortion techniques which primarily reduce the signal PAPR by clipping the time-domain GFDM signal. These strategies wouldn't perform well enough for PAPR reduction in GFDM systems due to their distortion properties and high error propagation rates [11]. Signal scrambling is another variety of PAPR reduction technology which includes Selective Mapping (SLM) and Partial Transmit Sequences (PTS) [12]. To generate numerous GFDM alternative signals, the GFDM signal is multiplied with random phase rotation vectors in the frequency domain in SLM. Following the inverse fast Fourier transform (IFFT), the alternative GFDM signal with the lowest PAPR is selected for transport. The candidate signal's side information (SI) is subsequently delivered, allowing for effective receiver recovery [13]. The PAPR is lowered in PTS techniques by dividing the signal into discontinuous subblocks, multiplying each subblock by an appropriate phase sequence vector, and afterward reconstituting the subblocks to produce a signal with a decreased PAPR [14]. Both the methods PTS and SLM are computationally demanding and need a search strategy for suitable phase sequence vectors. Furthermore, they necessitate providing the required phase sequence vectors with additional side information to the receiver, which decreases the system's spectral efficiency [15]. The majority of all the aforementioned PAPR mitigation solutions, however, exhibit poor performance in reducing PAPR and need an additional mechanism for constructing the alternative candidate signals for every bit stream. The final category of PAPR reduction strategies comprises precoding techniques including Discrete Hartley Matrix Transform (DHMT), Discrete Sine Matrix Transform (DSMT), and Discrete Cosine Matrix Transform (DCMT) [11]. Such techniques result in decreased PAPR because they reduce the aperiodic autocorrelation quantity amongst modulated data signals just before IFFT computation. Precoding techniques are one of the effective strategies to lower PAPR in GFDM systems. However, compared to signal scrambling techniques, their PAPR decrease is inferior.

Numerous PAPR reduction approaches have been discussed in the literature to alleviate the unacceptable high PAPR in GFDM systems. According to the authors of [16], the PAPR can be reduced for GFDM, OFDM, and SC-FDM by modifying the pulse shape used on sub-carriers. Zhang et al. [4] developed GFDM-aided NOMA schemes and evaluated their theoretical BER performance, concluding that the PAPR approach outperformed the OFDM technique. A data-independent precoder to reduce PAPR by lowering the variability of the instantaneous power while also retaining the average instantaneous power is presented

in [17] by compromising BER performance. In order to simplify the deployment of GFDM systems, Farhang et al. [18] suggested a technique founded on fast Fourier transform (FFT) usage and modulation matrices sparsification and could successfully decrease the computational complexity. Bandari et al. [19] suggested a Root Raised Cosine (RRC) filter-based wavelet-based PAPR reduction strategy in GFDM systems and demonstrated that wavelets effectively replace the traditional FFT operation in GFDM. Liu et al. [20] proposed an optimum pulse shaping-based PAPR reduction approach, although the authors were able to successfully lower the PAPR, the deviation of the filter coefficients actually increased the PAPR in the GFDM systems. To our knowledge, there has been little research on PAPR reduction in GFDM adopting improved precoding techniques. This idea persuaded us to carry out this research and propose an optimal approach for PAPR mitigation in GFDM systems using a precoding matrix.

In this paper, we propose an efficient PAPR reduction method based on precoding techniques, as well as an optimal orthogonal precoding matrix based on singular value decomposition (SVD) that possesses the least potential average power and a reasonably good PAPR minimization when compared to other existing precoding strategies without compromising PAPR reduction. We have reduced average power as well as the peak-to-average power ratio in an effort to enhance PAPR mitigation efficiency. Utilizing hardware from National Instruments (NI) known as the universal software radio peripheral (USRP), the authors develop a real-time prototype of the GFDM system to validate the idea of PAPR reduction. The received spectral response from USRP authenticates the proposed method by showing a good agreement with simulations.

The remaining part of the article is structured as follows: The standard GFDM transceiver model is described in Section II, and the methods for optimizing the precoding scheme to minimize average power, peak samples affixing, and experimental validation of the GFDM system's PAPR reduction are presented in Section III. Section IV compares the conventional and proposed systems and focuses on simulated and real-time outcomes. Lastly, Section V provides conclusions regarding the analysis that was conducted.

II. SYSTEM MODEL

The GFDM system is having a rectangular grid with K subcarriers and M time slots amounting to a total of $N = K \times M$ elements. The independent complex quadrature amplitude modulation (QAM) data is represented with $d_m(k)$ with $m = 0 \cdots M - 1$ and $k = 0 \cdots K - 1$, while $\mathbf{d} = [\mathbf{d_0^T} \ \mathbf{d_1^T} \cdots \mathbf{d_{M-1}^T}]^T$ represents the grid of data symbols. Here $\mathbf{d_m} = [d_m(0) \ d_m(1) \cdots d_m(K - 1)]$ represents the data on subsymbol and T in the superscript shows the transpose operation. An application desired prototype filter $g(n)$ extending for a long length of MK is used to perform circular convolution for combating OOB emissions. Finally, the

GFDM modulated signal is given by,

$$x(n) = \sum_{m=0}^{M-1} g\langle n - mK \rangle_N \underbrace{\sum_{k=0}^{K-1} d_m(k) e^{j\frac{2\pi kn}{K}}}_{\text{M copies of IDFT data}}$$

$$= \sum_{k=0}^{K-1} \sum_{m=0}^{M-1} d_m(k) g\langle n - mK \rangle_N \, e^{j\frac{2\pi kn}{K}} \quad (1)$$

where $\langle . \rangle$ is representing the modulo operation in order to obtain GFDM signal, $\mathbf{x} = [x_0 \cdots x_{MK-1}]$ and $n = 0, 1, \cdots N - 1$. The choice of circular prototype filter $g(n)$ clearly influences various performance metrics like bit error rate (BER) and PAPR, as presented in [21]. In this work, we use root raised cosine (RRC) filters as prototyping filters, whose auxiliary function can be represented in its simplified as [22],

$$G(f) = \sqrt{\frac{1}{2} [1 - \cos(\pi f(\beta))]} \quad (2)$$

The function $f(\beta)$ is defined on the roll-off function by varying alpha in the parameter $\beta = k/(\text{alpha} \times K)$. Here alpha can be considered as a measure for overlap between k^{th} subcarrier centered around normalized frequency k/K. Mathematically, the truncated Meyer auxiliary function is defined as,

$$f(\beta) = \beta^4 \left(35 - 84\beta + 70\beta - 20\beta^3 \right) \quad (3)$$

In simplified matrix representation (1) gets simplified into [18],

$$\mathbf{x} = \mathbf{Ad} \quad (4)$$

Matrix $\mathbf{A}$ is considered as modulation matrix, which consists of all the signal processing steps like upsampling, subcarrier filtering, frequency translation and $\mathbf{d}$ is the data vector. The transmitter vector $\mathbf{x_{cp}}$ is obtained as $\mathbf{x_{cp}} = [\mathbf{x}(MK - N_{cp} + 1 : MK); \mathbf{x}]$ after attaching N_{cp} samples at the start of the packet. The PAPR of the GFDM signal can be formulated as,

$$\text{PAPR}\{\mathbf{x_{cp}}\} = \frac{\max\{|\mathbf{x}|^2\}}{\text{E}\{|\mathbf{x}|^2\}} \quad (5)$$

where $\text{E}\{.\}$ computes expectation, $|.|$ is modulus of the complex number $\mathbf{x}$, and max is representing the maximum value. It is important to notice that, the use of cyclic prefix didn't enhance the numerical value of PAPR [23]. The received signal after cyclic prefix removal can be expressed as

$$\mathbf{y} = \mathbf{Hx} + \mathbf{W} \quad (6)$$

where $\mathbf{H}$ is the channel circulant matrix of dimension $N \times N$, with its first column obtained by appending $N - J$ zeros as $[h(0) \cdots h(J-1) \, 0 \cdots 0]^T$, and $\mathbf{W}$ represents the receiver additive white Gaussian noise (AWGN). The received signal $\hat{\mathbf{y}}$ obtained after zero-forcing equalization, by assuming perfect channel estimation is,

$$\mathbf{y} = \mathbf{W_N^H} \Lambda^{-1} \mathbf{W_N} \hat{\mathbf{y}} = \mathbf{x} + \mathbf{W_N^H} \Lambda^{-1} \mathbf{W_N} \mathbf{W} \quad (7)$$

where $\mathbf{W_N}$ and $\mathbf{W_N}^H$ represent N point fast Fourier transform (FFT) and inverse fast Fourier transform (IFFT) matrices, Λ is representing the eigenvalues obtained by using DFT of the first column of channel matrix $\mathbf{H}$. Here $\mathbf{W_N^H} \Lambda^{-1} \mathbf{W_N}$ in (7) is indicating the inverse channel response decomposed by using the circulant matrix property. As a result, the final detected signal is,

$$\mathbf{y} = \mathbf{x} \hat{+} \mathbf{H}^{-1} \mathbf{W} \quad (8)$$

We designed the receiver filter using the matched filter in order to maximize the signal-to-noise ratio (SNR) and the data symbols are obtained after multiplying with receiver matrix $\mathbf{A_r}$. Hence, the estimated data $\hat{\mathbf{d}}$ is,

$$\hat{\mathbf{d}} = \mathbf{A_r} \hat{\mathbf{y}} \quad (9)$$

Since $\mathbf{A_r}$ is designed using matched filter operation, $\mathbf{A_r} = \mathbf{A^H}$, where H is hermitian of a matrix. In the real-time transmission of GFDM signal using USRP, the receiver is sensitive to the presence of symbol time offset (STO) and carrier frequency offset (CFO). To compensate for this misalignment, a windowed preamble is added at the start of every transmission packet. We used the same preamble i.e., 44 length barker sequence for correction of time and frequency misalignment in indoor channel environments. It is a conventional practice in the IEEE 802.11 standard to use barker sequences as preamble sequences. The received signal with all the mentioned effects can be represented as,

$$y(n) = e^{j\frac{2\pi \epsilon n}{N}} \sum_{j=0}^{J-1} \sum_{n=0}^{N-1} h_n x_{j-n-\theta} + W(n) \quad (10)$$

The signal from the air would have an STO of θ and frequency shift factor ϵ along with additive white Gaussian noise (AWGN) $W(n)$. In this paper, we focus only on PAPR and spectral response of the transmitted signal and the details of the implementation of GFDM can be found in [24] and [25].

III. PROPOSED METHOD

The precoding-based techniques have a lot of potential because they are straightforward linear procedures that can be used without any additional side information. Neither substantially adding complexity nor disrupting the orthogonality of subcarriers, precoding enhances PAPR reduction performance. In this article, optimal precoding is taken into account as a method of lowering the PAPR of GFDM-transmitted signals. Before GFDM modulation and transmission, precoding in GFDM systems entails multiplying the modulated data of every GFDM block by a precoding matrix. The GFDM system uses a predetermined precoding matrix, so there is no requirement for a handshake between of transmitter and receiver. It will also be unnecessary to do all the processing required by block-based optimization techniques if the precoding matrix is the same for all GFDM frames. A novel process for effective precoding systems is suggested and examined here. To do so, the whole work is divided into three parts. A) Precoding matrix optimization for reducing

average power B) Affixing peak samples to GFDM signal for reducing both the average and peak power C) Experimental validation of the GFDM system's PAPR reduction.

A. PRECODING MATRIX OPTIMIZATION FOR REDUCING AVERAGE POWER

In the proposed technique, we design an optimal precoding matrix to reduce the average power, which also reduces PAPR. Assume that data d was generated after QAM mapping and then the data stream is segmented into blocks of size N. Then, a $N \times N$ matrix P precodes each block, known as a symbol vector. The GFDM signal after precoding can be expressed as:

$$X = PAd \quad (11)$$

where P denotes the designed precoding matrix, A is the GFDM modulation matrix, and d is the data vector. As mentioned earlier, the first step is to minimize the average power which is why this optimal matrix P is considered in such a way that the average power of (11) is minimized. The average power P_A is given as

$$\begin{aligned} P_A &= E[(PAd)^H PAd] \\ &= E[d^H A^H P^H PAd] \\ &= E[d^H (PA)^H PAd] \end{aligned} \quad (12)$$

Because the data's power is variable, if we wish to reduce the average power of (12), we must minimize the power contained in the PA matrix. Hence we decompose the PA matrix by using standard singular value decomposition as

$$PA = USV^H \quad (13)$$

where U and V are two unitary matrices of dimensions $N \times N$, i.e., $U^H U = I_K$ and $V^H V = I_N$, respectively, and S is a $N \times N$ diagonal matrix containing the singular values of PA on the diagonal, that is, $S_{i,i} = \sigma_i(PA)$. The distance between two consecutive discrete frequencies should be very low to offer fine resolution in an optimal frequency region for spectrum analysis, and hence the number of discrete frequencies, K, should be quite large. As a result, we suppose $K > N$. Also, keep in mind that rank $[PA] = N$. We derive (12) by substituting (11) and (13) as

$$P_A = E[d^H VS^H SV^H d] = \sum_{i=0}^{N-1} E[\left|[V^H d]_i\right|^2]\sigma_i^2(PA) \quad (14)$$

where $V^H d$ is an orthogonal transformation of d that has no effect on the Frobenius norm [26], because $(V^H d)^H V^H d = d^H d$. In general, any projection of a random variable vector d with identically distributed elements should have the same distribution. As a result, we assume that all of the projections' mean square values are consistent. With this premise, we have $E[\left|[V^H d]_i\right|^2] = P_s$, where P_s is the average power of each of the symbols in d. Therefore, (14) can be written as

$$P_A = P_s \sum_{i=0}^{N-1} \sigma_i^2(PA) = P_s \|PA\|^2 \quad (15)$$

Using Eckart-Young low-rank approximation theorem [27], [28] the precoding matrix can be optimized to reduce the average power of the GFDM signal. The minimum value of PA is given as

$$min \| PA \|^2 = \sum_{i=R}^{M-1} \sigma_i^2(P) \quad (16)$$

Rewriting the above equation

$$\| PA_{opt} \|^2 = \sum_{i=R}^{M-1} \sigma_i^2(P) \quad (17)$$

The optimal precoding matrix is provided as

$$P_{opt} = argmin \| PA \| \quad (18)$$

Further simplifying the above equation

$$PA = P_s \sum_{i=R}^{M-1} \sigma_i^2(P) \quad (19)$$

The matrix A is then decomposed using SVD to provide

$$SVD(A) = [U, S, V] \quad (20)$$

where U and V are unitary matrices with dimensions of $K \times K$ and $N \times N$, respectively. S is a diagonal matrix organized in decreasing order of all the singular values of A, i.e)., $\sum_{i,j} = \sigma_i(A)$ The Forbenius [26] minimum will be

$$min \| PA \| = \sqrt{\sum_{0}^{M-1} \sigma_i(P)} \quad (21)$$

The optimal precoding matrix to accomplish the least norm is derived by decomposing A utilizing SVD into $A = U_A S_A V_A^H$.

$$P_{opt} = QV_1 \quad (22)$$

where Q is an arbitrary $N \times N$ unitary matrix and V_1 is a $M \times N$ submatrix of V_A, consisting of the final N columns in V_A that correspond to the fewest N singular values. The average power substantially decreases when P_{opt} is multiplied by the GFDM data, yet the peak-to-average power remains ratio high. The peak-to-average power ratio will be decreased by adding peak samples to the GFDM signal in the next subsection.

B. AFFIXING PEAK SAMPLES TO GFDM SIGNAL FOR REDUCING BOTH THE AVERAGE AND PEAK POWER

As contrast to other conventional PAPR reduction strategies, which raise the average power or decrease the peak power of the GFDM signal, we are aiming to reduce PAPR by lowering both the average and peak power. By adding extra samples at the peaks of the pulse shaping function, the resulting signal has a smoother frequency spectrum with lower sidelobes. This is especially useful in circumstances with stringent spectrum limits or in multi-user systems where spectral resources

must be efficiently shared [29]. In the transmitter part, the proposed system comprises two blocks as shown in Fig. 2. The first is the peak samples identification (PSI), and the second is the samples affixing device (SAD). Peak sample identification and affixing is a technique that involves taking the peak L samples of a signal $x(n)$ with N samples and adhering them to the original signal to form a new signal $x(m)$ with $N + L$ samples in total. The L peaks are obtained from the GFDM signal as given in the following expression.

$$\{x_i\}_{i=1}^{L} = \underset{\{x_n^{(i)}(n)\}}{arg\ max}(\| \{x_n^{(i)}(n)\}_{n=0}^{N-i} \|) \tag{23}$$

To boost PAPR performance, we employ a strategy that adds peak L samples to the original GFDM sequence at the end of each GFDM frame, which increases average power and enhances PAPR performance. The newly generated precoded GFDM signal after adding L peaks can be expressed as

$$x_m(m) = \{x_n, <x_n>\} \begin{cases} \text{for } n = 0, 1, 2, \ldots, N-1 \\ \text{for } m = 0, 1, 2, \ldots, N+L-1 \end{cases} \tag{24}$$

Consider an OFDM symbol, for instance, with 256 subcarriers, or $N = 256$, and added top samples, or $L = 16$; this yields a time domain signal, $x_m(m)$, of 272 samples. The PAPR of the GFDM signal is then assessed both before and after adding peak samples. The original GFDM sequence's PAPR can be represented as:

$$PAPR(x_n) = \frac{max\ |x_n|^2}{\frac{1}{N}\sum_{n=0}^{N-1}|x_n^2|} \tag{25}$$

After adding peak samples to the GFDM sequence, PAPR can be changed as follows:

$$PAPR(x_m) = \frac{max\ |x_m|^2}{\frac{1}{M}\sum_{n=0}^{M-1}|x_m^2|} \tag{26}$$

Interestingly, the PAPR after adding peak samples to the GFDM signal is dramatically lowered, adding to the overall attractiveness of the strategy. The simulation results make the impact of the PAPR upon adding these peak samples quite evident. Finally, we receive a GFDM signal and then convert it to the original information signal in the receiving part. The final step is the counterpart to the transmitter portion, which is the same as the typical GFDM receiver, as well as the samples dissociate device (SDD) as shown in Fig. 2. The SDD section allows N + L samples at the input terminal and outputs N samples, i.e., SDD removes the bottom L samples from each GFDM symbol.

C. EXPERIMENTAL VALIDATION OF THE GFDM SYSTEM's PAPR REDUCTION

As described in previous sub-sections *A* and *B*, we first constructed an optimized precoding matrix for the GFDM system to reduce the average power, and then we selected fixed peak samples from the underlying GFDM sequence and

adjoined them to the end of each symbol to improve PAPR performance. As a result, by introducing peak samples, the average power is raised, and the overall ratio between peak power and average power is decreased. There is a trade-off between PAPR performance and the addition of peak samples to the GFDM signal, even though adding the peak samples improves PAPR performance. After adding the peak samples to the GFDM signal, we obtain the peaks in the signal's spectrum.

The power spectrum of the GFDM signal after adding peak samples is given as

$$|X_m(f)|^2 = \sum_{n=0}^{N-1}\sum_{k=0}^{N-1} x_n x_k e^{-j2\pi(f(n-k))/N} \tag{27}$$

When we include more peak samples in the GFDM signal, this will become much worse. We merely affix the number of peak samples for which the peak in the GFDM spectrum does not arise in order to avoid such intricacy. The impact of the spectrum when peak samples are added to the GFDM signal is explicated in the upcoming sub-section "Real-time results".

IV. RESULTS AND DISCUSSIONS
A. IMPLEMENTATION OF GFDM SYSTEM
The test bed used for the implementation of the concept of superimposed SI transmission is depicted in Fig. 1. LabVIEW is used as software, which can be easily amalgamated with national instruments hardware named universal software radio peripheral RIO. The primary attraction of LabVIEW is its simple reconfigurability without the use of additional hardware. USRP internally consists of a low-frequency daughter board for radio frequency translations, analog to digital converter (ADC)/digital-to-analog converter (DAC) for the development of the digital signal processing (DSP) chips inside the USRP. USRP is having the ability to operate in a wide frequency range of 1.2-6GHz, which covers all mobile communication scenarios. The major communication operations like digital up/down conversion and interpolation/decimation are implemented on the FPGA board of USRP, which is controlled by LabVIEW software for performing the baseband operations like modulation/demodulation. Hence, the actual FPGA implementation in the USRP is controlled by the software. This idea provides a chance to test the algorithm since the variations in software are replicated with implementation on hardware.

Fig. 1 clearly depicts two workstations, which are connected with a USRP using a NI PXIe-PCIe8371 express card. This interface is having a high throughput of $832MB/s$, which can be useful to exhibit real-time communication scenarios. After connecting the USRP a unique ID shall be assigned to the transmitter and receiver USRP. In LabVIEW, rectangular grid QAM modulated data is GFDM modulated on active subcarriers of the constituents in the order specified in the block diagram. After performing all baseband operations

FIGURE 1. Set up used for demonstrating real-time transmission of GFDM system.

Parameter	Value
Number of subsymbols	4
Number of subcarriers	64
Prototyping filter	Root raised
CP length	8
Transmitter oversampling factor	4
Filter roll-off factor	0.1
Preamble	44 length barker sequence
Receiver oversampling factor	4
Transmitter sampling rate	4M
Capture time	4ms
Receiver sampling rate	4M
Zero pad length	8
Receiver gain	1dB
Transmitter gain	0dB
Carrier frequency	6GHz

on the GFDM symbol a preamble and a zero sequence of length 8 are added at the start and end of each data packet [24]. The preamble is used to perform synchronization and channel estimation, while zero padding is useful to distinguish received signals in time. The packet transmitted in USRP not only contains payroll data but also control information. The control information consists of the USRP IP, the position of data with preambles, and error correction codes. Rx USRP receives the overlaid signal as a stream of data from free space. Rx USRP discards the data samples until significant energy is observed by using a detection algorithm. In other words, STO and CFO estimation is implemented and the detailed description can be found in [25]. Later, the channel impairments are equalized by estimating channel response using pilots.

B. SIMULATION RESULTS

This section explains the simulation results that were acquired using MATLAB software. The complementary cumulative density function ($CCDF$) is often used as a performance metric for measuring the PAPR (at $CCDF = 10^{-3}$). It is a measure of the probability of the PAPR of a GFDM signal exceeding a certain threshold level, $PAPR_0$. The GFDM system is simulated with 4-QAM modulation and the implementation parameters are detailed in Table 1.

The hardware implementation and subsequent reduction in costs rely on PAPR mitigation in any GFDM system. According to the proposed approach, the average power is decreased by including certain finite peak samples in the GFDM system after the optimum precoding matrix is created for GFDM systems. The proposed GFDM method is compared to the PAPR of average power changes for several existing techniques. Fig. 3 depicts the average power PAPR plot for various precoding-based PAPR reduction strategies compared to our methodology. The proposed approach is extremely low PAPR when compared to methods that use the Zadoff-Chu Transform (ZCT), the Walsh Hadamard Transform (WHT), and the Discrete Fourier Transform (DFT). The WHT and DFT have nearly identical PAPRs of roughly 33.5dB, however, the ZCT has a PAPR of 15.25dB. The proposed method's PAPR is only 3dB, and this level of PAPR reduction performance outperforms the traditional PAPR reduction schemes.

Fig. 3 shows a significantly reduced average power; in this Fig., we focus on lowering the peak-to-average power of the entire GFDM system by adding peak samples. The PAPR after adding specific peak samples to the GFDM is presented in Fig. 4. In the proposed scheme, comparisons are done for a wide range of peak sample values ranging from 8 to 64. The average power is initially lowered when the peak sample count is increased by 8 and then begins to grow when the peak sample count is increased further. In the GFDM system, the CCDF is only 3dB when no peak samples are introduced and grow to 4.2dB when peak samples reach 64. The PAPR for peak samples 16, 32, and 64 is between the two specified values.

The PAPR for the GFDM system is calculated before adding peak samples. Fig. 5 shows the PAPR performance of the designed precoding matrix and the existing techniques. We adopted the ZCT, WHT, and DFT to compare with the proposed method. The proposed approach has a PAPR of 8.9, which is approximately equal to the WHT. The ZCT has the highest PAPR of all the curves in Fig. 5, while the DFT has the lowest. We attach peak samples to the GFDM system in order to significantly reduce the PAPR of the proposed approaches. The PAPR performance of the proposed method is poor in this form of GFDM signal, but it improves when peak samples are attached, as illustrated in Fig. 6.

After adding peak samples to the GFDM, CCDF is measured and plotted as shown in Fig. 6. Without adding any peak samples, the suggested technique's PAPR performance is compared to that of adding peak samples counts 8, 16, 32, and 64. The PAPR for the curves with peak samples of 64, 32, 16, and 8 is 7.8, 7.8, 8, and 8.2 correspondingly. This PAPR reduction performance outperforms all of the previous approaches examined in this paper.

In GFDM, the roll-off factor is a parameter that controls the bandwidth of the pulse-shaping filter used in the transmitter. A higher roll-off factor results in a wider bandwidth pulse shaping filter, which reduces the ISI and improves the signal quality. However, a wider bandwidth pulse shaping
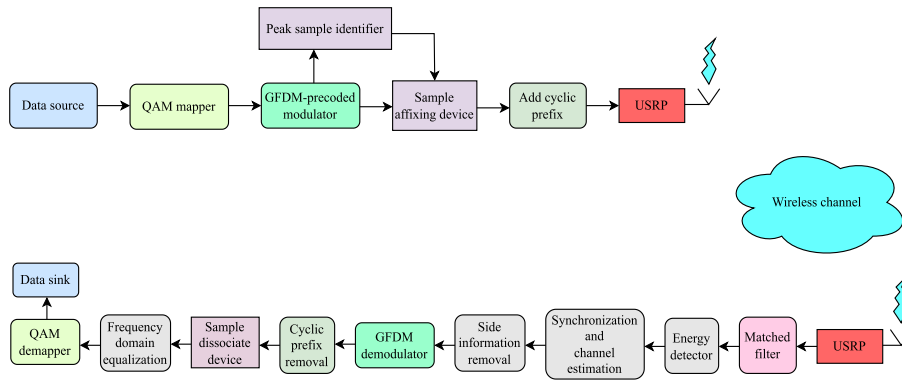
FIGURE 2. Block diagram for GFDM-precoding modulator with national instruments hardware USRP.
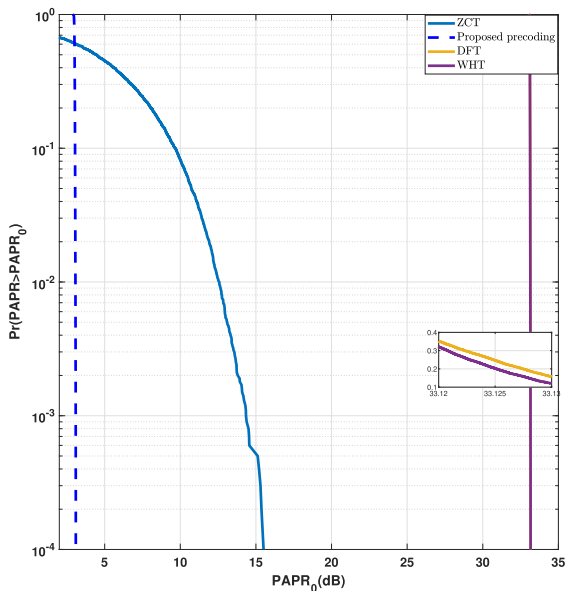

FIGURE 3. Comparing the average power of several precoding methods with the proposed method.
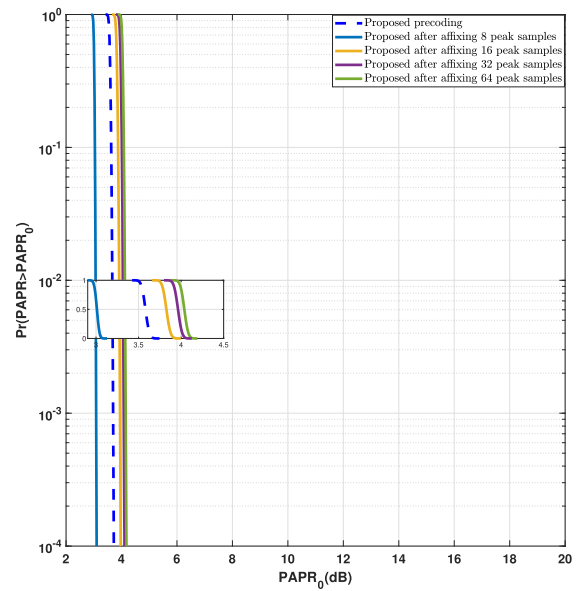

FIGURE 4. Comparison of the average power after attaching peak samples to the GFDM signal.

filter also increases the spectral leakage between adjacent subcarriers, which can lead to increased interference and reduced spectral efficiency [2]. Fig. 7 depicts the impact of various roll-off levels on the GFDM waveform's PAPR performance. It is well known that the PAPR rises as the GFDM signal's roll-off levels increase. The roll-off factor considered here is 0.9 and peak samples are added to the GFDM signal as shown in Fig. 7. In comparison to the curve without any addition of peak samples, the PAPR increased slightly when 8 peak samples were added to the GFDM signal. The PAPR is reduced for peak sample counts of 16, 32, and 64 when compared to the curve without any peak sample enhancements. However, when the roll-off factor is increased to the GFDM signal, the overall PAPR rises. As a result, when there is a balance between the number of peaks and the PAPR performance, this scheme will be the best PAPR reduction scheme among all PAPR reduction techniques.

C. REAL TIME RESULTS

As with the MATLAB simulation findings, we were able to acquire real-time results for the proposed GFDM system. The proposed precoding technique's power spectrum, as well as the precoding technique's result with the inclusion of peak samples, are produced for the GFDM system. We initially showed the power spectrum in Fig. 8 for the GFDM system using USRPs without any addition of peak samples.

To minimize the PAPR by increasing the average power, a finite amount of peaks are gathered from the input GFDM system and then attached at the end of each GFDM frame. The power spectrum is generated after adding several ranges of peaks to the proposed GFDM system. The implications of the proposed GFDM's PAPR performance when 8 peak samples from the input GFDM signal are shown in Fig. 9.

The power spectrum of the GFDM could be generated as in Fig. 10 if the peak samples are raised to 16. When the peak sample count surpasses 16, the power spectrum of the GFDM
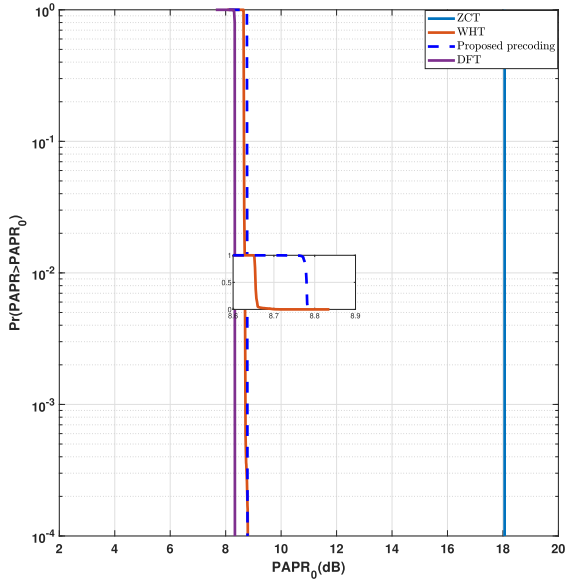
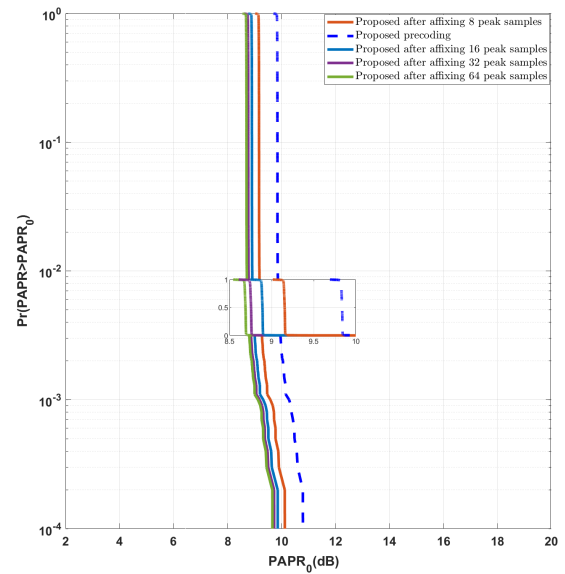**FIGURE 5.** PAPR plot of designed precoding matrix versus existing approaches.

FIGURE 6. PAPR comparison of designed precoding matrix after peak sample introduction.

FIGURE 7. PAPR plot of the designed matrix after adding peak samples with roll-off factor 0.9.

FIGURE 8. Received spectrum with perfect SI transmission.

FIGURE 9. Received spectrum with number of Top samples 8.
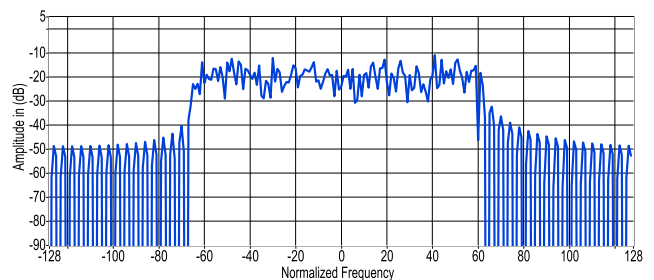
FIGURE 10. Received spectrum with number of Top samples 16.

will have a spike, which can be problematic at the transmitter. As a result, the number of peak samples should be carefully chosen in order to avoid such spikes in the GFDM signal's power spectrum.

If more peak samples are added to the GFDM signal, the spectrum will contain a huge spike, which might be indicative of how the GFDM hardware should be designed. In Fig. 11, when 32 peak samples are added to the GFDM signal to lower the PAPR, this effect is clearly seen. However, we can observe, as the P value decreases, the received spectral response gradually approaches the ideal response in Fig. 11. It can be inferred from the previous discussion
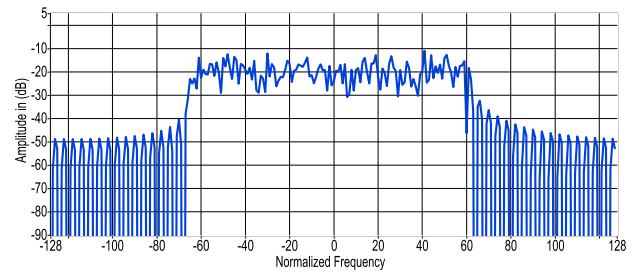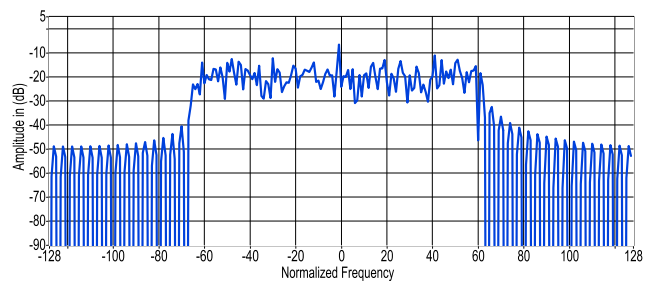
that, as P decreases we achieve better PAPR and spectral response at the cost of BER. Since only a few peaks of the
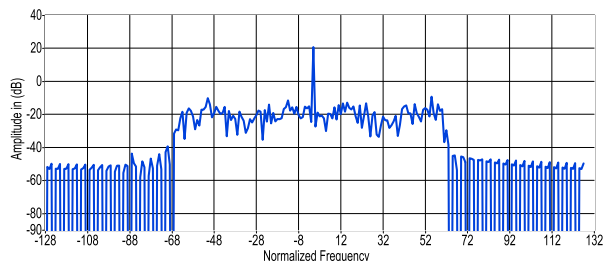
FIGURE 11. Received spectrum with number of Top samples 32.

GFDM signal are added to the original GFDM signal, the BER performance is only minimally impacted.

V. CONCLUSION

Therefore, the proposed method improves data efficiency as well as PAPR and makes the GFDM system an enticing alternative for 5G communication. The optimization challenge of designing a precoding matrix with the lowest PAPR is addressed. In addition to refining the precoding matrix, this paper discusses a creative method for improving PAPR by adding peak samples to the original GFDM signal. According to simulation results, the precoding strategy can significantly reduce the PAPR in GFDM systems. The robustness of the experimental and simulation results provides credibility to the proposed PAPR reduction technique in GFDM systems.

ACKNOWLEDGMENT

REFERENCES

[1] Y. Li, K. Niu, and C. Dong, "Polar-coded GFDM systems," *IEEE Access*, vol. 7, pp. 149299–149307, 2019.

[2] M. Murad, I. A. Tasadduq, and P. Otero, "Towards multicarrier waveforms beyond OFDM: Performance analysis of GFDM modulation for underwater acoustic channels," *IEEE Access*, vol. 8, pp. 222782–222799, 2020.

[3] Y. Kim, H. Lee, M. Matthé, G. Fettweis, and H. J. Yang, "GFDM-based asynchronous grant-free multiple-access," *IEEE Access*, vol. 10, pp. 31012–31030, 2022.

[4] X. Zhang, Z. Wang, X. Ning, and H. Xie, "On the performance of GFDM assisted NOMA schemes," *IEEE Access*, vol. 8, pp. 88961–88968, 2020.

[5] L. Dai, Z. Wang, and Z. Yang, "Time-frequency training OFDM with high spectral efficiency and reliable performance in high speed environments," *IEEE J. Sel. Areas Commun.*, vol. 30, no. 4, pp. 695–707, May 2012.

[6] F. Li, K. Zheng, L. Zhao, H. Zhao, and Y. Li, "Design and performance of a novel interference-free GFDM transceiver with dual filter," *IEEE Trans. Veh. Technol.*, vol. 68, no. 5, pp. 4695–4706, May 2019.

[7] E. Güvenkaya, E. Bala, R. Yang, and H. Arslan, "Time-asymmetric and subcarrier-specific pulse shaping in OFDM-based waveforms," *IEEE Trans. Veh. Technol.*, vol. 64, no. 11, pp. 5070–5082, Nov. 2015.

[8] S. K. Bandari, V. M. Vakamulla, and A. Drosopoulos, "Novel hybrid PAPR reduction schemes for the MGFDM system," *Phys. Commun.*, vol. 31, pp. 69–78, Dec. 2018.

[9] S. Weinstein and P. Ebert, "Data transmission by frequency-division multiplexing using the discrete Fourier transform," *IEEE Trans. Commun. Technol.*, vol. COM-19, no. 5, pp. 628–634, Oct. 1971.

[10] A. Goel, P. G. Poddar, and M. Agrawal, "A novel quadrilateral companding transform for PAPR reduction in OFDM systems," *Digit. Signal Process.*, vol. 85, pp. 113–123, Feb. 2019.

[11] Z. Fang, H. Qian, K. Kang, H. Wang, and Y. Jin, "Distortion-less PAPR reduction algorithm for multi-user MIMO system with linear precoding," *Digit. Signal Process.*, vol. 95, Dec. 2019, Art. no. 102575.

[12] Y. Yuan, S. Wei, X. Luo, Z. Xu, and X. Guan, "Adaptive PTS scheme based on fuzzy neural network for PAPR reduction in OFDM system," *Digit. Signal Process.*, vol. 126, Jun. 2022, Art. no. 103492.

[13] S. Valluri and V. V. Mani, "A novel approach for reducing complexity in the SLM-GFDM system," *Phys. Commun.*, vol. 34, pp. 188–195, Jun. 2019.

[14] M. S. Ahmed, S. Boussakta, A. Al-Dweik, B. Sharif, and C. C. Tsimenidis, "Efficient design of selective mapping and partial transmit sequence using T-OFDM," *IEEE Trans. Veh. Technol.*, vol. 69, no. 3, pp. 2636–2648, Mar. 2020.

[15] S.-Y. Zhang and B. Shahrrava, "A SLM scheme for PAPR reduction in polar coded OFDM-IM systems without using side information," *IEEE Trans. Broadcast.*, vol. 67, no. 2, pp. 463–472, Jun. 2021.

[16] N. Michailow and G. Fettweis, "Low peak-to-average power ratio for next generation cellular systems with generalized frequency division multiplexing," in *Proc. Int. Symp. Intell. Signal Process. Commun. Syst.*, Nov. 2013, pp. 651–655.

[17] Z. Sharifian, M. J. Omidi, H. Saeedi-Sourck, and A. Farhang, "Linear precoding for PAPR reduction of GFDMA," *IEEE Wireless Commun. Lett.*, vol. 5, no. 5, pp. 520–523, Oct. 2016.

[18] A. Farhang, N. Marchetti, and L. E. Doyle, "Low-complexity modem design for GFDM," *IEEE Trans. Signal Process.*, vol. 64, no. 6, pp. 1507–1518, Mar. 2016.

[19] S. K. Bandari, V. M. Vakamulla, and A. Drosopoulos, "PAPR analysis of wavelet based multitaper GFDM system," *AEU, Int. J. Electron. Commun.*, vol. 76, pp. 166–174, Jun. 2017.

[20] K. Liu, W. Deng, and Y. Liu, "Theoretical analysis of the peak-to-average power ratio and optimal pulse shaping filter design for GFDM systems," *IEEE Trans. Signal Process.*, vol. 67, no. 13, pp. 3455–3470, Jul. 2019.

[21] J. Wu, X. Ma, X. Qi, Z. Babar, and W. Zheng, "Influence of pulse shaping filters on PAPR performance of underwater 5G communication system technique: GFDM," *Wireless Commun. Mobile Comput.*, vol. 2017, pp. 1–7, Feb. 2017.

[22] J. T. Dias and R. C. de Lamare, "Unique-word GFDM transmission systems," *IEEE Wireless Commun. Lett.*, vol. 6, no. 6, pp. 746–749, Dec. 2017.

[23] A. D. S. Jayalath and C. Tellambura, "SLM and PTS peak-power reduction of OFDM signals without side information," *IEEE Trans. Wireless Commun.*, vol. 4, no. 5, pp. 2006–2013, Sep. 2005.

[24] S. P. Valluri and V. V. Mani, "Investigation of blind CFO estimation for GFDM system using universal software radio peripheral: Theory, simulations and experiments," *IET Commun.*, vol. 13, no. 13, pp. 1936–1944, Aug. 2019.

[25] S. P. Valluri and V. V. Mani, "Demonstration of effect of oversampling on jitter removal for multitaper GFDM system using SDR," in *Proc. Int. Conf. Adv. Technol. Commun. (ATC)*, Oct. 2018, pp. 168–173.

[26] G. H. Golub and C. F. Van Loan, *Matrix Computations*, 3rd ed. Baltimore, MD, USA: The Johns Hopkins Univ. Press, 1996.

[27] L. Hogben, *Handbook of Linear Algebra*, L. Hogben, Ed. Boca Raton, FL, USA: CRC Press, 2007.

[28] D. S. Bernstein, *Matrix Mathematics: Theory, Facts, and Formulas*, 2nd ed. Princeton, NJ, USA: Princeton Univ. Press, 2009.

[29] J. Ji, G. Ren, and H. Zhang, "PAPR reduction in coded SC-FDMA systems via introducing few bit errors," *IEEE Commun. Lett.*, vol. 18, no. 7, pp. 1258–1261, Jul. 2014.

SIVAPRASAD VALLURI was born in Hyderabad, Telangana, India, in 1990. He received the B.Tech. degree in electronics and communication engineering from GITAM University, Vishakhapatnam, India, in 2011, the M.Tech. degree in communication engineering from NIT Surat, Gujarat, India, in 2016, and the Ph.D. degree in wireless communication from NIT Warangal, India, in 2019.

He is currently an Assistant Professor of electronics and communication engineering with the Indian Institute of Information Technology Design and Manufacturing, Kurnool, India. He has been teaching a wide range of subjects and establishing laboratories in VLC systems. He has more than 11 publications in various international journals and conferences. His research interests include mobile communications, wireless communications, and visible light communications.

CHAKRAVARTHY GUNTURU received the B.Tech. degree in electronics and communication engineering from Jawaharlal Nehru Technological University, Hyderabad, India, and the M.Tech. degree in communication and signal processing from Acharya Nagarjuna University, Guntur, India. He is currently pursuing the Ph.D. degree in visible light communications with the Indian Institute of Information Technology Design and Manufacturing, Kurnool, India.

SOWBHAGYA APPALLA is currently pursuing the bachelor's degree in electronics and communication engineering with the Indian Institute of Information Technology Design and Manufacturing, Kurnool, India. Her research interests include non-linear methods in the reduction of PAPR and communication systems.

ANUPAM KAJALE is currently pursuing the bachelor's degree in electronics and communication engineering with the Indian Institute of Information Technology Design and Manufacturing, Kurnool, India. His research interest includes precoding methods in the reduction of PAPR in GFDM systems.

V. V. MANI (Senior Member, IEEE) received the B.E. and M.E. degrees in electronics and communication engineering from the College of Engineering, Andhra University, India, in 1992 and 2003, respectively, and the Ph.D. degree in electrical engineering from the Indian Institute of Technology Delhi, India, in 2009. She joined the Electronics and Communication Engineering Department, NIT Warangal, in April 2008, as an Assistant Professor, where she has been a Professor, since July 2022. She has numerous publications in credit in national and international conferences and journals. Her research interests include wireless communication and signal processing for communication. She is a fellow of the Institute of Electronics and Telecommunication Engineers (IETE), India.

• • •